PCCP

Diffusion in Li2O studied by Non-Equilibrium Molecular Dynamics for 873 < T/K < 1603

SCHOLARONE™
Manuscripts

PAPER

Diffusion in Li$_2$O studied by Non-Equilibrium Molecular Dynamics for 873 < T/K < 1603†

Alexander D. Mulliner,[a] **Philippe C. Aeberhard,**[b] **Peter D. Battle,**[a] **William I. F. David**[a,b] **and Keith Refson**[b,c]

The use of non-equilibrium molecular dynamics facilitates the calculation of the cation diffusion constant of Li$_2$O at temperatures too low to be accessible by other methods. Excellent agreement with experimental diffusion coefficients has been obtained over the temperature range 873 < T/K < 1603. Diffusion below 1200 K was shown to be dominated by a concerted nearest-neighbour hopping process, whereas in the high-temperature superionic region an additional mechanism involving a six-coordinate interstitial cation site in the anti-fluorite structure becomes increasingly dominant. Our model thus accounts for the transition from the superionic regime to the non-superionic regime.

1 Introduction

Lithium oxide, Li$_2$O, is one of the simplest binary compounds of lithium. It adopts the face-centred cubic anti-fluorite struc-

[a] *Department of Chemistry, Inorganic Chemistry Laboratory, University of Oxford, South Parks Road, Oxford OX1 3QR, United Kingdom. E-mail: alex.mulliner@chem.ox.ac.uk, peter.battle@chem.ox.ac.uk*
[b] *ISIS Facility, Rutherford Appleton Laboratory, Chilton, Oxfordshire, OX11 0QX, United Kingdom*
[c] *Deptartment of Physics, Royal Holloway, University of London, Egham, TW20 0EX, United Kingdom*

† Electronic Supplementary Information (ESI) available. Movies of diffusion events extracted from NEMD simulations of Li$_2$O. The black dots represent the trace of the Li$^+$ cations throughout the movie. Movie 1: 490 ps trace of one Li$^+$ cation (green) diffusing through the oxide sublattice (red) at 973 K. Here and in movie 2 the lower part of the movie shows a projection down [010], the upper part is projected down [100] and each point on the trace represents a time window of 200 fs. Movie 2: 490 ps trace of one Li$^+$ cation (green) diffusing through the oxide sublattice (red) at 1373 K. Movie 3: A 2 ps section of movie 1 showing the concerted nearest-neighbour mechanism. Here and in movie 4 the green sphere is the Li$^+$ cation seen in movie 1, blue spheres represent neighbouring Li$^+$ cations and each point on the trace represents 2 fs. Movie 4: A 1.6 ps section of movie 1 showing the octahedral interstitial mechanism operating in the low temperature regime. Movie 5: A 5 ps section of movie 2 showing the octahedral interstitial mechanism operating in the high-temperature regime. The movie also includes a ⟨110⟩ hop. The green sphere is the Li$^+$ cation seen in movie 2 and the blue spheres represent neighbouring Li$^+$ cations. The purple trace represents Li$^+$ ions that do not hop during the movie, but are shown for completeness. Each point on the trace represents 2 fs.

ture with Li$^+$ ions occupying the tetrahedral interstitial sites at $\left(\frac{1}{4}, \frac{1}{4}, \frac{1}{4}\right)$ in a close-packed array of oxide ions; each of the anions is thus coordinated by a cubic arrangement of eight Li$^+$ cations; the edges of this cube are parallel to those of the unit cell (Fig. 1a). A vacant interstitial site, coordinated by six O^{2-} anions, lies at the centre of the unit cell (Fig. 1b).
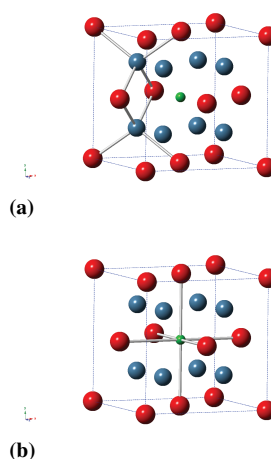
Fig. 1 The unit cell of Li$_2$O; red and blue circles represent oxygen and lithium, respectively. The (a) tetrahedral coordination of lithium and edge-sharing of adjacent tetrahedra and (b) octahedral coordination of the interstitial site, represented by a green circle at $\left(\frac{1}{2}, \frac{1}{2}, \frac{1}{2}\right)$, are shown.

At elevated temperatures Li$_2$O behaves as a superionic conductor, with Li$^+$ cations exhibiting very high diffusivity rates through the static oxide framework: the self-diffusion coefficient of the oxide ions is approximately five orders of magnitude lower than that of the lithium ions and the electronic conductivity is negligible.[1,2] The use of Li$_2$O in composite glass-ceramic and polymer-ceramic electrolytes in Li-air batteries[3] resulted in an improvement in the conductivity and long-term stability of the electrolytes[4,5] and the oxide has consequently been extensively investigated using a range of experimental methods.[6,7] Specifically, the lithium diffusion coefficients have been determined over a wide range of temper-

ature by Oishi et al.[1,2] Their data show an increased temperature dependence of the diffusion coefficient in the so-called superionic region above 1273 K. The observed diffusion rate is too high to be solely attributable to the low concentration of Frenkel defects found in Li_2O and some form of concerted mechanism is likely to operate.[8,9]

Cation diffusion in Li_2O above 1300 K has also been the subject of many computational studies[10–19] and Hayoun et al.[13,14] have identified multiple mechanisms that operate in the superionic regime. However, our knowledge of the ionic diffusion pathways and the mechanisms that lie behind the behaviour observed at temperatures below and around the transition from the non-superionic to the superionic regime is still limited. The *ab initio* computational methods used previously to study Li_2O fall into two main categories; Arrhenius descriptions of known or predicted pathways[10–12] and the utilization of the Einstein-Sutherland relation to extract diffusion coefficients from molecular dynamics (MD) simulations.[13–17] Of the two, MD is the preferred method as it does not assume any prior knowledge of diffusion pathways and intrinsically accounts for many-particle effects. However, the limits of *ab initio* MD are the system size (hundreds of atoms) and the accessible time scale (10-100 ps), which is frequently much smaller than the timescale typical of hopping events in the diffusion process. Consequently the number of diffusion events typically observed in MD simulations is very few or nil, making the determination of diffusion coefficients inaccurate at best. This mismatch of timescales limits the use of equilibrium MD to liquids and superionic solids at very high temperatures. In the specific case of Li_2O, equilibrium MD simulations are inadequate for studies of diffusion except at temperatures close to the melting point, where the rate of diffusion is very high; for example Fracchia et al.[15] and Pfei et al.[16] were unable to reproduce the observed lithium diffusion below 1300 K.

In order to probe low-temperature diffusion accurately, non-equilibrium molecular dynamics (NEMD) can be used. A NEMD simulation increases the rate of hopping events observed in a predictable manner, thus diffusion coefficients under equilibrium conditions can be determined for systems in which very few or no diffusion events would be observed in equilibrium MD simulations. NEMD was originally developed to study transport phenomena in model liquids[20] and has recently been used to study lithium-ion diffusion in solid $LiBH_4$.[21] In the NEMD method a fictitious external field is applied to the diffusing species. This has the effect of increasing the frequency of rare hopping events and consequently the rate of diffusion is accelerated. The fictitious external field, called the colour field,[22] is conceptually similar to an electric field in that the displacement of the colour-labeled species parallel to the applied field is linearly proportional to the field strength. The particle flux in the applied colour field is evaluated during

the simulation and the diffusion coefficient is then computed using linear response theory. As the colour field strength increases from zero, the response is initially linear, but when the colour field becomes too strong, nonlinear effects begin to dominate. In the linear regime, any process observed can be mapped directly onto an equilibrium process; beyond this regime it can not.

In this work we have modeled the diffusion of lithium in Li_2O using NEMD; a few equilibrium MD calculations were also carried out for comparison purposes. Both classical force field (FF) and density functional theory (DFT) models were used for the simulations, in conjunction with the classical equations of motion. The former allows the use of much larger supercells and, more significantly, longer simulation times than the latter because it is much more computationally efficient. FF also allows for the comparison of diffusion coefficients from simulations with and without colour fields present. Our simulations of Li_2O yield diffusion coefficients that compare well with the experimental data. The use of NEMD has also enabled us to probe for the first time the mechanistic detail of the diffusion process below, as well as above, the superionic transition and hence to identify and establish the relative importance in different temperature regimes of the multiple diffusion pathways that are available. This demonstrates the potential of NEMD for the analysis of diffusion in solids.

2 Computational Details

The simulations presented in this work were performed on a supercell consisting of 128 formula units (384 atoms) in a 2x2x8 array of cubic unit cells with periodic boundary conditions. The lattice parameters used at all temperatures were determined previously in neutron single-crystal diffraction experiments.[6] At these experimental densities the simulated dynamic pressures were ± 2.5 GPa. Preliminary studies showed that the unidirectional diffusion in response to the colour field allows for the use of an anisotropic supercell without biasing the computed diffusion coefficients. Evidence from test calculations on 4x4x8 and 2x2x12 supercells, performed at 1273 K, showed finite size errors in the Li diffusion coefficients of less than 14%. However, for super cells smaller than 2x2x8, finite-size effects led to inflated lithium diffusion coefficients because the Li^+ ions then experience significant interactions with their own periodic image. In the case of FF-NEMD and DFT-NEMD, the colour field was applied along [001] with alternating (010) sheets of Li^+ cations being assigned +1 and -1 colour charge. The [001] direction was chosen because it gave the largest response in test calculations which also considered $\langle 110 \rangle$ and $\langle 111 \rangle$.

The MD simulation package CP2K,[23] modified[21] to include the colour diffusion algorithm, was used for all the simulations. The temperature was controlled by the Gaussian isoki-

netic thermostat.[22] The equations of motion were integrated with a time step of 2 fs, in order to minimize the drift of the conserved quantities. The DFT-NEMD simulations used the Quickstep method[24] with the Perdew-Burke-Ernzerhof functional.[25] The valence electrons were represented with a double-zeta Gaussian basis set[26] with a 280 Ry cutoff energy for the plane waves, and the core electrons by Goedecker-Teter-Hutter pseudopotentials.[27] The classical force-field simulations used the Buckingham potential (Eqn. 1) with the parameters A, C and ρ determined by Fracchia et al.[15] for Li_2O.

$$V(r) = \frac{q_1 q_2}{r} + A \exp\left(\frac{-r}{\rho}\right) - \frac{C}{r^6} \qquad (1)$$

The duration of the NEMD simulations was 50 ps and 500 ps for DFT and classical force fields, respectively. The colour fields were applied after an initial equilibrium was established.

3 Results and Discussion

Li_2O was initially simulated at 1273 K with three different computational methods: DFT-NEMD, FF-NEMD, and FF-MD. The method outlined in Aeberhard et al.[21] was used to extract the diffusion coefficients from the NEMD simulations and the Einstein-Sutherland relation was used in the case of the MD simulations. For reasons that will be explained below, FF-NEMD was then used to calculate the diffusion coefficient as a function of temperature. Simulations were performed at six further temperatures: 873, 973, and 1123 K, which are in the non-superionic regime, and 1373, 1473, and 1603 K, which are in the superionic regime.

Table 1 Lithium self-diffusion coefficients obtained from different computational methods at 1273 K. The experimental result obtained from Oishi et al.[1] was measured at 1312 K.

Method	$\log D_{Li} / cm^2 s^{-1}$	Simulation time / ps
FF-MD	-5.96 ± 0.05	500
FF-NEMD	-6.18 ± 0.03	500
DFT-NEMD	-6.02 ± 0.08	50
Oishi et al.	-6.23	-

The agreement between the three calculated values and the experimental diffusion coefficient at 1273 K is very good, see Table 1, and demonstrates the transferability of the potential parameters determined by Fracchia et al.[15] However there were differences in the efficiency of the three different computational methods; DFT-NEMD requires high-performance computing resources whereas FF-NEMD can be run on a personal computer. As a consequence of the lower computational cost per timestep, FF-NEMD permits the use of much longer simulation times, more thorough sampling of the linear regime and, when necessary, the use of a significantly larger supercell.
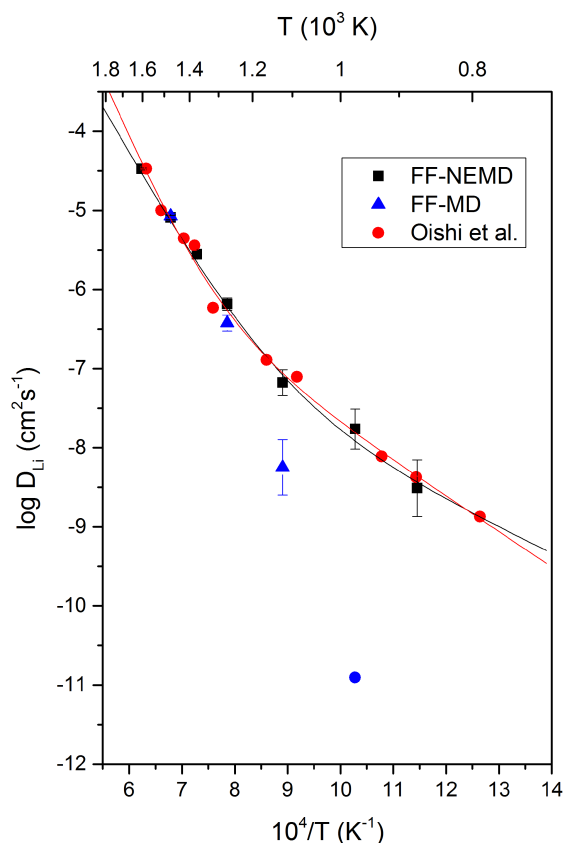
Fig. 2 Temperature dependence of the Li^+ diffusion coefficient in Li_2O. Red circles represent values from Oishi et al.[1]; black circles represent values from FF-NEMD simulations; blue triangles and the blue circle represent values from FF-MD simulations. The red and black lines are fits to Eqn. 2 for the experimental and FF-NEMD simulated data, respectively.

Consequently many more hopping events were observed, thus substantially reducing the error in the diffusion coefficient extracted. The use of the colour diffusion algorithm does not affect the computational time per MD step, which is therefore the same in FF-MD as in FF-NEMD. However the number of hopping events is significantly fewer without the colour field, which again led to a larger error in the diffusion coefficient. FF-NEMD is thus the better method for this study and the results obtained by this method will be presented and discussed below. We emphasise that the diffusion coefficient and the mechanistic details determined at 1273 K by DFT-NEMD and FF-MD were consistent with those determined by FF-NEMD, but with lower levels of precision.

The temperature dependence of the diffusion coefficient de-

rived from FF-NEMD and FF-MD simulations is shown in Fig. 2. The results of the FF-NEMD simulations agree well with the experimental data throughout the measured temperature range, even though the diffusion coefficient varies by four orders of magnitude. The FF-MD calculations agree with experiment above 1250 K, but not at lower temperatures. In both cases, as the simulation temperature decreases the number of diffusion-related hopping events decreases and the error in the calculated diffusion coefficient increases. In the case of the FF-MD calculations at 973 K, no diffusion events took place during the simulation. A value of $\log D_{Li} \sim 10^{-11} \, cm^2 s^{-1}$ calculated by FF-MD is thus indistinguishable from zero and the data point plotted as a blue circle in Fig. 2 is only included to provide an indication of the sensitivity limit of the method.

The experimental curve and that calculated using FF-NEMD both show an increase in gradient as the temperature increases above ~1273 K. When interpreted using an Arrhenius model this implies a change in activation energy and thus a change in the underlying lithium diffusion mechanism or a change in the relative importance of different mechanisms if more than one is present. Comparison of diffusion traces covering an interval of 490 ps at 973 K, see Fig. 3a and Movie 1†, and 1373 K, see Fig. 3b and Movie 2†, illustrates the change in the nature and rate of the macroscopic cation displacement. The FF-NEMD trajectories were therefore examined to elucidate the mechanistic detail of local lithium hopping in both the superionic and the non-superionic regimes. In the non-superionic regime hopping is comparatively infrequent and usually proceeds via a direct hop between nearest-neighbour (nn) sites along the $\langle 100 \rangle$ directions (Fig. 3a). Each individual hop occurs along one direction with little movement in the two perpendicular directions; we shall return to this point below. Four neighbouring Li sites, forming a closed loop, were involved in all the events we observed. This is illustrated in Movie 3† for one of the events seen in Movie 1†. This mechanism is observed at all temperatures simulated. The concerted nature of this hopping removes the need for a cation vacancy to initiate the movement. In addition to the nn hopping around a closed loop, a limited amount of hopping initiated by the movement of a cation along $\langle 111 \rangle$ to the octahedral interstitial site at $(\frac{1}{2}, \frac{1}{2}, \frac{1}{2})$ is observed at low temperatures. This movement creates a vacancy on the lithium sublattice that allows $\langle 100 \rangle$ hops between adjacent sites to occur. In the low temperature region four regular sites are involved before the interstitial cation returns along a $\langle 111 \rangle$ direction to a regular site, thus terminating the process [Movie 4†]. The maximum residence time for a cation in the interstitial site at 973 K is 400 fs. As the simulation temperature is increased this mechanism begins to dominate the interstitial-free process. Furthermore, the number of cations moving during each event increases from 4 to, typically, 12 or 14 as the maximum interstitial residence time increases to 4 ps. While the interstitial site is occupied

(a)

(b)
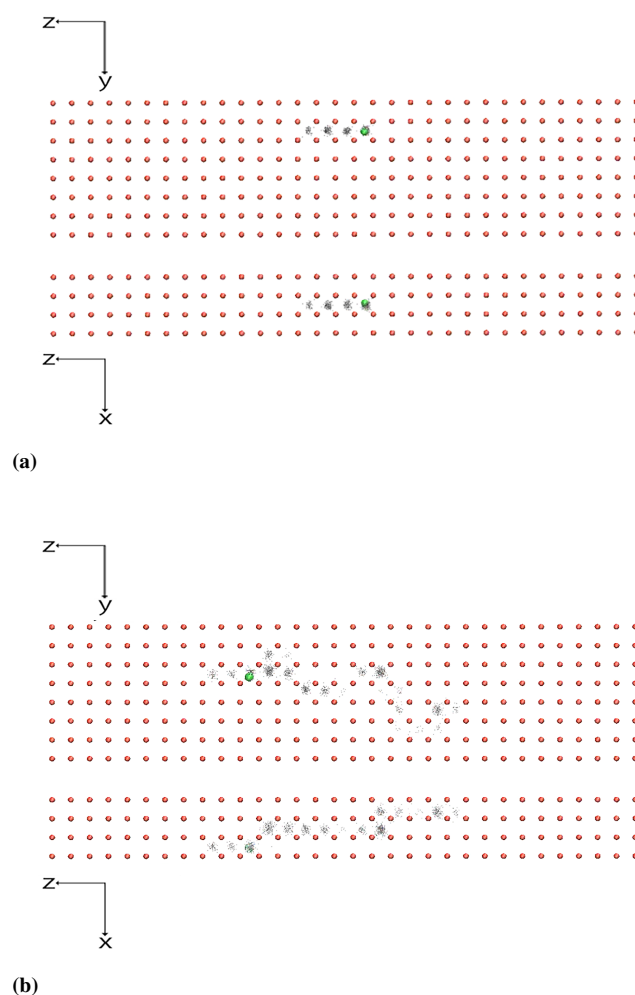
Fig. 3 Traces showing diffusion of one Li^+ cation (green) through the oxide sublattice (red), over a time of 490 ps (a) at 973 K and (b) at 1373 K. The upper (lower) part of both (a) and (b) is projected along [100] ([010]). Each point in the trace represents a time window of 200 fs.

Table 2 Parameters derived in fitting experimental and simulated diffusion coefficients to Eqn. 2

Method	FF-NEMD	Oishi et al.
k_1	-4.81 ± 0.13	-3.25 ± 0.13
k_2	2.91 ± 0.80	5.43 ± 0.80
$\Delta E_1 \,/\, \text{kJ mol}^{-1}$	26.9 ± 1.5	37.2 ± 1.0
$\Delta E_2 \,/\, \text{kJ mol}^{-1}$	100 ± 6.7	134 ± 6.7

the movement of the lithium ions principally consists of $\langle 100 \rangle$ hops, although a small number of $\langle 110 \rangle$ hops are also observed. Movie 5† shows the detailed operation of this process during a 5 ps section of the macroscopic diffusion process illustrated in Movie 2†.

Our calculations show that the diffusion in the superionic regime is largely dependent on the interstitial mechanism, with the concerted process making a smaller contribution. The reverse situation is observed in the low-temperature regime. This is consistent with the results of a neutron diffraction study[6] that revealed a rapid increase in the occupancy of the interstitial site above 1200 K. We have fitted the experimental and simulated diffusion coefficients to the function:

$$\log D_{Li} = \log\left(\exp\left[k_1 - \frac{\Delta E_1}{k_B T} \right] + \exp\left[k_2 - \frac{\Delta E_2}{k_B T} \right] \right) \quad (2)$$

where the subscripts 1 and 2 correspond to the nn and octahedral-interstitial diffusion mechanisms, respectively. The resulting values of ΔE_i, the activation energy for each mechanism, and k_i, a measure of the corresponding attempt frequency, are tabulated in Table 2 and the excellent fit quality achieved across the measured temperature range is shown in Figure 2. The values of k_1 and k_2 are consistent with the observation that the octahedral-interstitial mechanism becomes more important at higher temperatures as the ratio $\Delta E_i/k_B T$ decreases. The ratio $\Delta E_1/\Delta E_2$ is consistent with the cation having to pass between three anions forming the face of an oxide octahedron when making a [111] hop, rather than between the two anions forming the edge of an octahedron during a [100] hop. This is discussed in more detail below. Although the agreement between the diffusion coefficients measured by Oishi et al. and those calculated by FF-NEMD appears excellent, the fitting parameters derived from the two curves differ significantly. This reflects the sensitivity of the fit to the parameterisation used. For example, we recognise that our two-mechanism fit neglects the relatively small number of [110] hops observed at high temperature.

Figure 4(a) shows the coordinates of a lithium cation as it makes a nn [001] hop. In order to make such a hop the cation must pass between two oxide ions that are separated by a distance $a_0/\sqrt{2}$, i.e. 3.25 Å. This suggests that the Li – O dis-
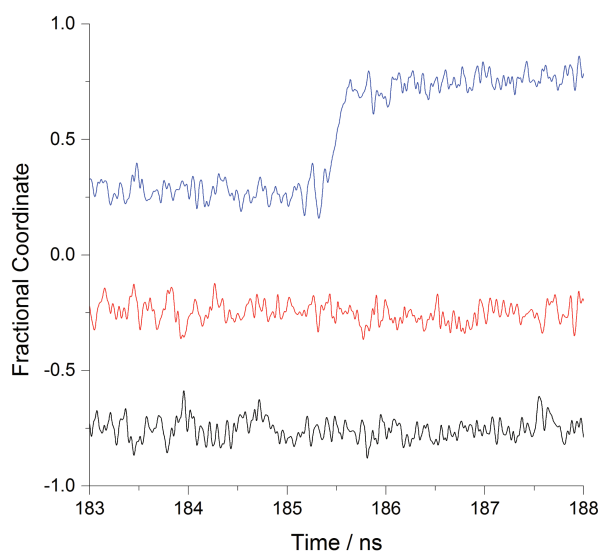
(a)
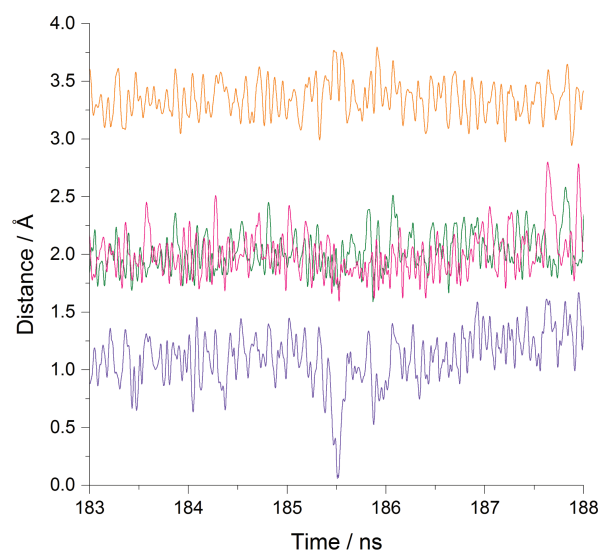
(b)

Fig. 4 The trajectories of a Li$^+$ cation at 973 K simulated with FF-NEMD; (a) the black, red, and blue lines represent the x, y, and z fractional coordinates, respectively, of the cation for the nn mechanism along [001]. (b) The orange line shows the separation of the two oxide ions between which the cation passes. The pink and green lines show the two lithium-oxygen distances. The purple line shows the distance between the cation and the instantaneous midpoint of the two oxide ions.
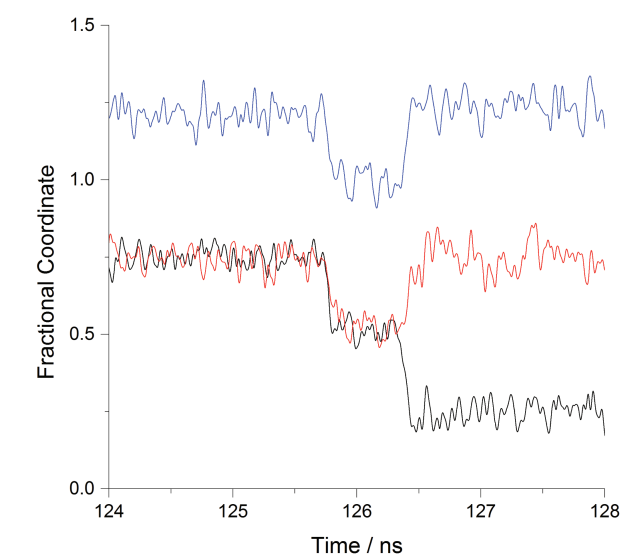
(a)
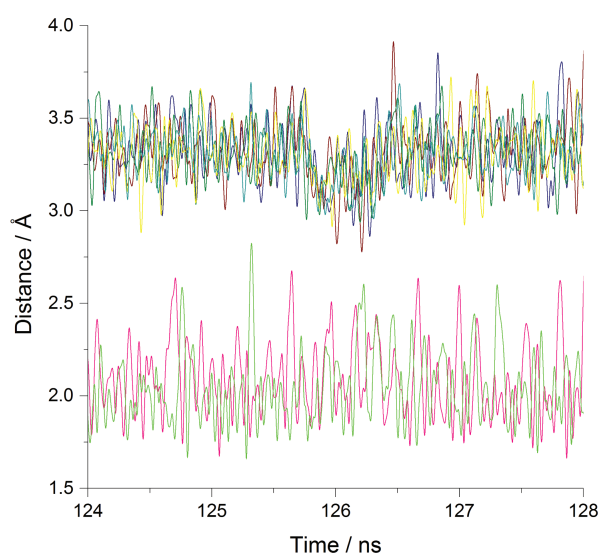
(b)

Fig. 5 The trajectories of a Li$^+$ cation at 1273 K simulated with FF-NEMD; (a) the black, red, and blue lines represent the x, y and z fractional coordinates, respectively, of the cation as it follows the octahedral-interstitial mechanism along $[\bar{1}\bar{1}\bar{1}]$ to the interstitial site, then along $[\bar{1}11]$ to the final site; (b) The yellow, navy, dark red and olive lines show the oxygen-oxygen distances around the interstitial site. The pink and green lines show the Li - O distances in the triangular window through which the cation passes.

tance might be reduced to a chemically unreasonable value during the course of the hop. We therefore studied the time dependence of the O – O and Li – O distances more closely, see Figure 5(b), and found that the lithium does not travel along a linear path; there is some limited movement in the plane perpendicular to the direction of the hop. The cation passes close to, but not through, the instantaneous midpoint of the O – O vector. In this way the interatomic distances are maintained at, or very close to, their equilibrium values. The average minimum distance between the diffusing cation and the midpoint of the O – O vector is 0.017(12) Å and the lowest observed value was 0.0059 Å. In the case of a [111] hop, see Figure 5(a), the cation must pass through an equilateral triangle formed by three oxide ions in order to reach the six-coordinate interstitial site. The variation of the Li – O distances during that process is shown in Figure 5(b). It can be seen that when one Li – O distance becomes unusually short another increases in order to reduce overcrowding; i.e. the pink and green lines in Fig. 5(b) are not in phase. The Li – O distance around the interstitial site in an undistorted fluorite structure would be $a_0/2 \sim 2.3$ Å, which is somewhat longer than the distance of 2.08 Å found in other oxides[28] containing six-coordinate lithium. In order to address this under-bonding the oxide ions are displaced during the period when the interstitial site is occupied, see Figure 5(b), so that the mean Li – O distance is reduced to 2.14 Å; the mean O – O separation decreases from 3.33 to 3.19 Å. It is perhaps surprising that the oxide sublattice does not show a more significant response to other components of the cation motion.

4 Conclusions

We have calculated the diffusion coefficient of the Li$^+$ ion in Li$_2$O with a high degree of precision in both the superionic and non-superionic temperature regimes. The excellent agreement at all temperatures in the range $873 < T/K < 1603$ between our calculated values and the experimental data surpasses that obtained in previous studies[13–17,19] which were only able to consider the high-temperature regime. The atomic trajectories produced by the NEMD simulations, which were analyzed in order to provide mechanistic detail of the Li$^+$ diffusion, revealed that both a nearest-neighbour mechanism and an octahedral-interstitial mechanism operate at all temperatures although their relative contribution changes; the nn mechanism dominates at low temperatures and the interstitial mechanism at high temperatures. The latter induces a response from the oxide sublattice that has not been recognised in previous studies. The increased significance of the octahedral-interstitial mechanism above the transition to the superionic regime accounts for the increased temperature dependence of the diffusion coefficient compared to that in the low temperature regime. Our success stems from the ability of

NEMD to model the simultaneous operation of multiple diffusion mechanisms over a wider temperature range than has previously been possible. This method allowed simulations to be performed not only with more computational efficiency than would have been achievable with equilibrium MD methods, but also down to lower temperatures where the slow rate of diffusion reduces the precision and efficacy of the latter methods. The mechanisms were determined by the NEMD simulations without the use of bias or prior knowledge of diffusion pathways. These results demonstrate the value of FF-NEMD methods in the study of solid-state electrochemical devices that operate outside the superionic regime.

References

1 Y. Oishi, Y. Kamei and M. Akiyama, *Journal of Nuclear Materials*, 1979, **87**, 341–344.

2 M. Akiyama, K. Ando and Y. Oishi, *Solid State Ionics*, 1981, **4**, 3–6.

3 B. Kumar, J. Kumar, R. Leese, J. P. Fellner, S. J. Rodrigues and K. M. Abraham, *Journal of the Electrochemical Society*, 2010, **157**, A50.

4 B. Kumar, D. Thomas and J. Kumar, *Journal of the Electrochemical Society*, 2009, **156**, A506.

5 J. Kumar, S. J. Rodrigues and B. Kumar, *Journal of Power Sources*.

6 T. W. D. Farley, W. Hayes, S. Hull, M. T. Hutchings and M. Vrits, *Journal of Physics: Condensed Matter*, 1991, **3**, 4761.

7 K. Noda, A. Shluger, T. Nakazawa, Y. Ishii and N. Itoh, *Nuclear Instruments and Methods in Physics Research*, 1994, **91**, 307–311.

8 A. De Vita, I. Manassidis, J. S. Lin and M. J. Gillan, *EPL (Europhysics Letters)*, 1992, **19**, 605.

9 A. De Vita, M. J. Gillan, J. S. Lin, M. C. Payne, I. Stich and L. J. Clarke, *Physical Review Letters*, 1992, **68**, 3319–3322.

10 Y. Duan and D. C. Sorescu, *Physical Review B*, 2009, **79**, 014301.

11 R. Dovesi, C. Roetti, C. Freyria-Fava, M. Prencipe and V. Saunders, *Chemical Physics*, 1991, **156**, 11 – 19.

12 J. Rodeja, M. Meyer and M. Hayoun, *Modelling and Simulation in Materials Science and Engineering*, 2001, **9**, 81.

13 M. Hayoun, M. Meyer and A. Denieport, *Acta Materialia*, 2005, **53**, 2867–2874.

14 M. Hayoun and M. Meyer, *Acta Materialia*, 2008, **56**, 1366–1373.

15 R. Fracchia, G. Barrera, N. Allan, T. Barron and W. Mackrodt, *Journal of Physics and Chemistry of Solids*, 1998, **59**, 435–445.

16 J. Pfeiffer, H. Sanchez-Sanchez and L. J. Alvarez, *Journal of Nuclear Materials*, 2000, **280**, 295 – 303.

17 P. Goel, N. Choudhury and S. L. Chaplot, *Physical Review B*, 2004, **70**, 174307.

18 M. Hayoun and M. Meyer, *Surface Science*, 2013, **607**, 118–123.

19 M. K. Gupta, P. Goel, R. Mittal, N. Choudhury and S. L. Chaplot, *Physical Review B*, 2012, **85**, 184304.

20 E. J. Maginn, A. T. Bell and D. N. Theodorou, *Journal of Physical Chemistry*, 1993, **97**, 4173–4181.

21 P. C. Aeberhard, S. R. Williams, D. J. Evans, K. Refson and W. I. F. David, *Physical Review Letters*, 2012, **108**, 095901.

22 D. J. Evans, W. G. Hoover, B. H. Failor, B. Moran and A. J. C. Ladd, *Physical Review A*, 1983, **28**, 1016–1021.

23 *CP2K: released under the GPL license, freely available at http://www.cp2k.org*.

24 J. Van de Vondele, M. Krack, F. Mohamed, M. Parrinello, T. Chassaing and J. Hutter, *Computer Physics Communications*, 2005, **167**, 103–128.

25 J. P. Perdew, K. Burke and M. Ernzerhof, *Physical Review Letters*, 1996, **77**, 3865–3868.

26 J. Hutter, M. Parrinello and G. Lippert, *Theoretical Chemistry Accounts*, 1999, **103**, 124–140.

27 S. Goedecker, M. Teter and J. Hutter, *Physical Review B*, 1996, **54**, 1703.

28 P. D. Battle, C. P. Grey, M. Hervieu, C. Martin, C. A. Moore and Y. Paik, *Journal of Solid State Chemistry*, 2003, **175**, 20 – 26.